Difference-Based Image Noise Modeling Using Skellam Distribution

Youngbae Hwang, *Member*, *IEEE*, Jun-Sik Kim, *Member*, *IEEE*, and In So Kweon, *Member*, *IEEE*

Abstract—By the laws of quantum physics, pixel intensity does not have a true value, but should be a random variable. Contrary to the conventional assumptions, the distribution of intensity may not be an additive Gaussian. We propose to directly model the intensity difference and show its validity by an experimental comparison to the conventional additive model. As a model of the intensity difference, we present a Skellam distribution derived from the Poisson photon noise model. This modeling induces a linear relationship between intensity and Skellam parameters, while conventional variance computation methods do not yield any significant relationship between these parameters under natural illumination. The intensity-Skellam line is invariant to scene, illumination, and even most of camera parameters. We also propose practical methods to obtain the line using a color pattern and an arbitrary image under natural illumination. Because the Skellam parameters that can be obtained from this linearity determine a noise distribution for each intensity value, we can statistically determine whether any intensity difference is caused by an underlying signal difference or by noise. We demonstrate the effectiveness of this new noise model by applying it to practical applications of background subtraction and edge detection.

Index Terms—Difference-based noise modeling, Skellam distribution, edge detection, background subtraction.

1 Introduction

Noise is inevitable in any image-capturing process. Even though the statistical nature of quantum physics can primarily account for the source of the noise, most existing noise modeling methods in the computer vision community do not use its physical characteristics, but simply try to model noise in a probabilistic framework.

1.1 Motivation

In various computer vision tasks, such as edge detection, corner detection, and background subtraction, it is important to determine whether or not the intensities of two pixels come from the same scene radiance. Intensities that come from the same radiance may vary for a number of reasons, and this variation is called *image noise*.

Conventionally, pixel intensity has been simply modeled as a sum of *true* intensity and *additive* noise. For example, the previous approaches [1], [2], [3] use the additive noise model to represent the observed intensity, I, contaminated by image noise as

$$I = I_0 + \mathcal{N}(\mu, \sigma^2), \tag{1}$$

where I_0 is the *true* intensity and $\mathcal{N}(\mu, \sigma^2)$ is the distribution of noise with the mean μ, and variance σ^2. For the case of a Gaussian noise model, the mean μ is set to 0 and only the variance is used to estimate the noise distribution. For the case of a Poisson model, the noise $\mathcal{N}$ follows a zero mean Poisson noise assuming that the other sources are much smaller than shot noise [4]. Similarly to the Gaussian noise model, the mean is 0 and the variance is used to estimate intensity variation by image noise.

Fig. 1 shows the intensity distributions and their parameterized estimation using the conventional additive noise models. We captured a pattern image, as shown in Fig. 1a, and estimated the noise distribution by calculating the mean and variance of pixel intensities within a single patch. Fig. 1b shows the fitting results of a color channel for a patch using the Gaussian distribution and Poisson distribution. The measured intensity distributions are not even symmetric, and the estimation curves using the additive noise model do not fit to the real intensity distributions. When we use parameters from the erroneous modeling, the further processing based on them may fail to obtain reliable outputs. The characteristic of the *additive* noise model that is vulnerable to illumination effects causes this erroneous case. Because pixel intensity is governed by quantum physics, it cannot have a *true* value, but can only be considered to be a random variable.

Back to the original problem of determining whether or not two pixel intensity values correspond to the same scene radiance, it is required to compare two random variables of pixel intensity. Among the diverse approaches for comparing two random variables, we choose to directly model the distribution of intensity difference as a single random variable. The distribution of the *intensity differences* shown in Fig. 1c is more symmetric and easy to fit to a parameterized

- *Y. Hwang is with the Multimedia IP Center, Korea Electronics Technology Institute (KETI), #68 Yatap-dong, Bundang-gu, Seongnam-si, Gyeonggi-do 463-816, Korea. E-mail: ybhwang@keti.re.kr.*
- *J.-S. Kim is with the Robotics Institute, Carnegie Mellon University, 5000 Forbes Avenue, Pittsburgh, PA 15213. E-mail: kimjs@cs.cmu.edu.*
- *I.S. Kweon is with the Department of Electrical Engineering, KAIST, #3215 Electrical Engineering Building (E3), Guseong-dong, Yuseong-gu, Daejeon, Korea. E-mail: iskweon@ee.kaist.ac.kr.*

Manuscript received 6 May 2010; revised 14 Jan. 2011; accepted 10 Oct. 2011; published online 30 Nov. 2011.
Recommended for acceptance by S. Belongie.
For information on obtaining reprints of this article, please send e-mail to: tpami@computer.org, and reference IEEECS Log Number TPAMI-2010-05-0351.
Digital Object Identifier no. 10.1109/TPAMI.2011.224.

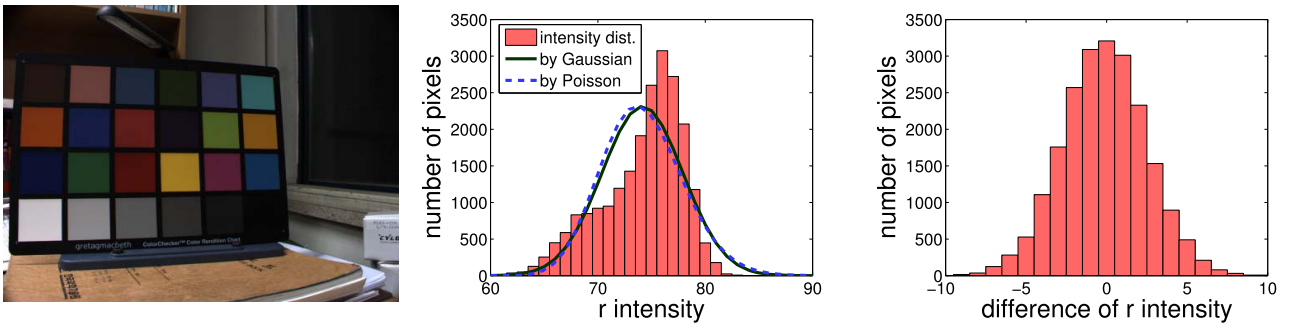

(a) Input image for noise modeling (b) Intensity distribution in R channel (c) Intensity difference distribution in R channel

Fig. 1. Histograms of intensity and intensity difference for a patch (15th patch). Conventional additive models do not explain the distribution well, while intensity difference modeling can explain the distribution better.

model. This example shows that the difference of intensity values follows a parameterized distribution better than the distributions of the intensity itself, which is usually assumed to follow an additive Gaussian or a Poisson distribution. The modeling of intensity difference makes it possible to statistically determine whether the difference is caused by an image noise or by a scene radiance change. In addition, we demonstrate that a noise model based on intensity difference can eliminate the effect of illumination, contrary to the conventional additive noise model.

1.2 Related Work

There have been studies that have endeavored to estimate image noise by analyzing the camera imaging process. Healey and Kondepudy [4] pointed out that there are five major noise sources, including shot noise, fixed pattern noise, and dark current noise. They described a calibration procedure that corrects for spatial nonuniformity caused by fixed pattern noise and by variation in dark current noise. They further insisted that the variance of the noise is linearly proportional to the intensity statistically. Their method requires hundreds of images for estimating sensor noise. Alter et al. [1] developed a noise model based on Poisson noise and quantization noise in low-light conditions. In their noise model, the mean and variance exhibit a relationship of exponentially decaying oscillation under low-light conditions which approaches linearity as intensity increases. They also derived an intensity similarity measure based on their noise model and showed improved matching accuracy.

Liu et al. [2], [3] recently proposed another noise estimation method from a single image. They defined a noise level function as a variation of the standard deviation of noise with respect to image intensity. After learning the noise level function, which describes how the noise level changes with brightness, they used Bayesian MAP estimation to infer the noise level function from a single image. They applied their noise model to bilateral filtering and Canny edge detection [3]. Because of their assumption that an image is piecewisely smooth, their method provides only the upper bounds of noise levels rather than the expected distribution of the noise. Hence, their noise estimation is inappropriate for measuring the intensity difference between two pixels. For Canny edge detection, their method only determines the higher threshold with Gaussian smoothing in a fixed scale. Therefore, their edge detector cannot take into account the per-pixel effect of image noise, which depends on brightness.

Foi et al. [5] recently presented a signal-dependent noise model which is composed of a Poissonian part for photon-counting process and a Gaussian part for the remaining stationary disturbances. They not only showed the derivation statistically, but also explained the relationship to elementary aspects of the digital sensor's hardware. In the main algorithm of noise modeling, they exploited the usual Gaussian approximation of the Poisson distribution, and thus their noise modeling can be regarded as an intensity-dependent Gaussian model. The authors mainly focused on estimating standard deviations according to intensity under the piecewise smoothness assumption as well. They did not apply the estimated noise model to further applications.

1.3 Contributions

We present three contributions in terms of noise modeling and its applications. First, we show that modeling of intensity difference is more accurate and useful than the conventional additive noise model using variance, as we briefly introduced before. In Section 2, a more detailed comparison between the two models will be provided, and it will show that the intensity difference modeling offers a more significant linear relation between the intensity and noise parameters than the conventional methods [1], [2], [3]. The proposed difference modeling is able to handle the illumination effects under natural lights without any local transformation based on color segmentation [2], [3].

Second, we propose to use a parameterized distribution model—Skellam distribution—as an intensity difference model. In Section 3, we derive it from the Poisson distribution of photons collected at a single pixel considering shot and dark current noise. Noise modeling based on a Skellam distribution has been used before in the context of PET imaging [6], but to the best of our knowledge it has not been applied to natural images. We also make comparisons between the exact Skellam modeling and its Gaussian approximation for intensity differences. The relation between the Skellam parameter and intensity is investigated in Section 4 in various setups of a camera, such as a CCD/CMOS sensor, gain, and exposure time, and we propose a simple method to obtain the parameter in a single natural image.

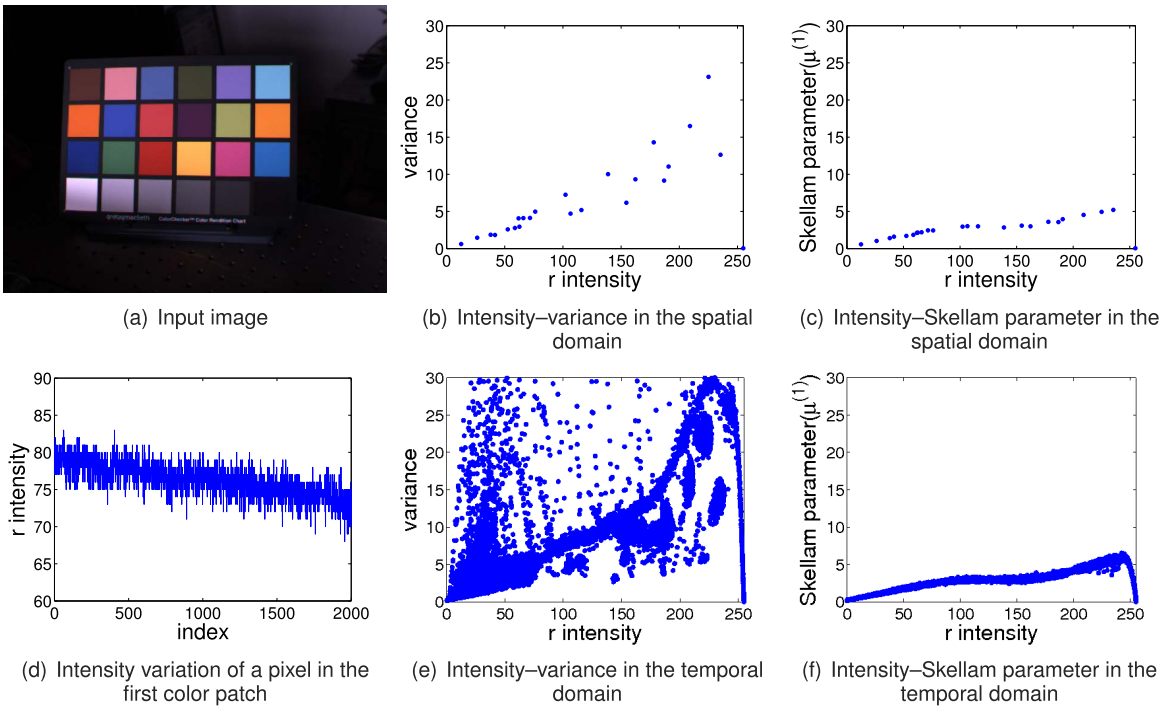

(a) Input image (b) Intensity–variance in the spatial domain (c) Intensity–Skellam parameter in the spatial domain

(d) Intensity variation of a pixel in the first color patch (e) Intensity–variance in the temporal domain (f) Intensity–Skellam parameter in the temporal domain

Fig. 2. Relationship between noise parameters and intensity in the temporal and spatial domains under natural illumination conditions. The statistic of intensity difference has a stronger relationship with intensity than the intensity variance, which is conventionally used.

Finally, we show that the proposed intensity difference model is useful for practical applications in Sections 5 and 6 in both temporal and spatial domains. Background subtraction and edge detection are transformed into the original problem of determining whether or not two pixel intensity values correspond to the same scene radiance, and the direct modeling of an intensity difference can handle it statistically.

The preliminary version of this paper appeared in [7]. In this version, we focus on the importance of *the modeling of intensity difference* whichever the underlying distribution is chosen by providing experimental results. In addition, we make a comparison between the proposed Skellam and Gaussian approximation, verify the proposed noise model for various CCD/CMOS cameras, and investigate the effect of camera settings, such as gain and exposure time. A new application in the temporal domain, background subtraction, is provided with quantitative evaluation.

2 Validity of Modeling Intensity Differences

In Fig. 1, we show that the intensity distributions are not explained well by the conventional additive noise model, while the intensity difference looks easier to model in a parameterized form. In this section, we make a comparison between the conventional model and a parameterized model which we will propose later. The additive noise model has been used to estimate the relationship between intensity and noise parameters in previous works [2], [3], [4], [5]. These works start from calculating variances of pixels from the same scene radiance. We first look into the meaning of the variance in the conventional noise modeling.

If one assumes that image noise η_e is additive and follows a Poisson distribution, intensity I is modeled as

$$\begin{aligned} I &= I_0 + \eta_e, \quad \text{where } \eta_e \equiv I_e - \mu, \\ I_e &\sim f_P(I_e \mid \mu) = \frac{\mu^{(I_e)} e^{-\mu}}{(I_e)!}, \end{aligned} \tag{2}$$

where I_0 is the true intensity and I_e follows a Poisson distribution with variance μ used to model the noise. The Poisson distribution is shifted by μ so that image noise η_e has zero mean. For a homogeneous patch P in which the sample mean of the pixel intensities is $\overline{I}$, we can derive the parameter μ by the variance of the intensities as

$$\mu = \frac{\sum_{(i,j)\in P} (\overline{I} - I(i,j))^2}{n-1}. \tag{3}$$

The conventional noise variance estimation used in the previous methods [1], [2], [3], [5] actually estimates the parameter of an additive Poisson noise model. Note that if the variance is large enough, the Poisson noise model can be approximated by a Gaussian distribution.

For the homogeneous patches in the ColorChecker image shown in Fig. 2a captured by a Point Grey Flea camera, we estimated the noise parameter of the Poisson distribution μ using (3), which is actually the variance of intensities in patches. As shown in Fig. 2b, it is difficult to find the relationship between variance μ and intensity. On the other hand, the Skellam parameter $\mu^{(1)}$ from *the intensity difference*, which we will explain in the later sections, has a strong linear relationship with intensity, as shown in Fig. 2c. The modeling of intensity difference shows a more significant relationship to intensity than conventional variance computation, or equivalently, the additive Poisson modeling does.

This is clearer when we see the statistics in the temporal domain. We captured 2,000 images under natural illumination conditions, as shown in Fig. 2a. As time went by, the intensity level decreased, as shown in Fig. 2d. In this case,

the intensity variances, conventionally used for noise modeling, are greatly scattered in the temporal domain, as shown in Fig. 2e, and it is hard to see any parametric relation between intensity and its variance. As shown in Fig. 2f, the relationship between the intensity and the parameter from the intensity difference is almost linear and the relationship in both the temporal and the spatial domains is preserved even under the variation in illumination conditions. These results show that the modeling of the intensity difference provides a more valid and consistent relationship than the conventional intensity variance between intensity and the noise parameters in both temporal and spatial domains.

3 Intensity Difference Model

Because the pixel intensity including image noise should be considered as a random variable, two random variables should be compared to determine whether or not two pixel intensity values correspond to the same scene radiance. In order to compare them, we model intensity difference directly as a single random variable.

3.1 Skellam Distribution of Intensity Differences

Throughout this paper, we assume a linear response camera whose intensity is linearly proportional to the number of photons collected at an imaging element. The number of photons received at a collection site (usually a particular pixel) is governed by the laws of quantum physics; thus it cannot have a *true* value, but should be described as a random variable. This variation is called *photon noise*. The probability distribution for n_e photons at a site during an observation of time interval T seconds is known to have a Poisson distribution [1], [4], [8]:

$$f_P(n_e \mid \rho, T) = \frac{(\rho T)^{n_e} e^{-\rho T}}{n_e!}, \tag{4}$$

where ρ is the rate parameter, measured in photons per second. The mean μ and the variance σ^2 of the distribution over an interval T in (4) are given by

$$\mu = \sigma^2 = \rho T. \tag{5}$$

It is obvious that the number of photons in a brighter pixel is greater than that in a darker pixel, and the expected number of photons μ will increase as brightness (or intensity) increases. We will show this in Section 4.1.

Three traditional assumptions about the relationship between signal and noise generally do not hold for dominant photon-dependent noise [8]: Image noise is 1) *not independent* of the signal, 2) *nor Gaussian*, 3) *nor additive*. Because the dominant photon-dependent noise is not additive, and the noise and *true* intensity of a pixel cannot be separated, we directly use the distribution of an intensity difference, rather than making an erroneous assumption of *additive* noise.

Here, we generalize our previous model [7] to consider all photon-dependent noise sources, including *dark current noise*. Dark current noise increases the number of photons independently of an input signal. Because the number of photons n_t generated by dark current noise also follows a Poisson distribution [8], we can write this distribution as

$$f_P(n_t \mid \mu_t) = \frac{(\mu_t)^{n_t} e^{-\mu_t}}{n_t!}, \tag{6}$$

where μ_t is the average number of photons resulting from dark current noise.

Note that the sum of two Poisson random variables also follows a Poisson distribution whose parameter becomes the sum of the parameters of the two Poisson random variables. Finally, the distribution of noise with respect to both photon noise and dark current noise can be expressed as

$$f_P(n_e \mid \mu_p + \mu_t) = \frac{(\mu_p + \mu_t)^{n_e} e^{-(\mu_p + \mu_t)}}{n_e!}, \tag{7}$$

where μ_p represents the number of photons produced by photon noise (or shot noise).

The difference between the two Poisson random variables follows a Skellam distribution [9]. The probability mass function (pmf) of a Skellam distribution is a function of $k = n_1 - n_2$, the difference between two Poisson random variables n_1 and n_2. The difference of the two Poisson random variables in (7), which is the distribution of the whole *photon-dependent* noise, can be written as

$$f_S\left(k; \mu_{pd}^{(1)}, \mu_{pd}^{(2)}\right) = e^{-\left(\mu_{pd}^{(1)} + \mu_{pd}^{(2)}\right)} \left(\frac{\mu_{pd}^{(1)}}{\mu_{pd}^{(2)}}\right)^{k/2} I_{|k|}\left(2\sqrt{\mu_{pd}^{(1)} \mu_{pd}^{(2)}}\right), \tag{8}$$

where $\mu_{pd}^{(1)} \equiv \mu_p^{(1)} + \mu_t^{(1)}$, $\mu_{pd}^{(2)} \equiv \mu_p^{(2)} + \mu_t^{(2)}$, and $I_k(z)$ denotes the modified Bessel function of the first kind.

In the special case that $\mu^{(1)} = \mu^{(2)}$, a Gaussian distribution approximates a Skellam distribution for sufficiently large μ and k [10]. However, a Gaussian distribution cannot approximate the Skellam distribution for low-intensity pixels because neither μ nor k is sufficiently large. If we can estimate $\mu_{pd}^{(1)}$ and $\mu_{pd}^{(2)}$ from a given set of intensity differences k, our noise model can consider the noise sources together in this single formulation. In the remainder of this paper, the subscript pd is omitted for simplicity.

3.2 Skellam Parameter Estimation

Under the assumption of a linear response camera, we can estimate the Skellam parameters from the statistics of intensity differences. The mean μ_S and variance σ_S^2 of a Skellam distribution are given by

$$\mu_S = \mu^{(1)} - \mu^{(2)},\ \sigma_S^2 = \mu^{(1)} + \mu^{(2)}. \tag{9}$$

From (9), we calculate the parameters $\mu^{(1)}$ and $\mu^{(2)}$ directly as

$$\mu^{(1)} = \frac{\mu_S + \sigma_S^2}{2},\ \mu^{(2)} = \frac{-\mu_S + \sigma_S^2}{2}. \tag{10}$$

The statistics μ_S and σ_S^2 are obtained as follows from each pixel in an image sequence of a static scene:

$$\mu_S = \frac{\sum_t (I_t(i,j) - I_{t+1}(i,j))}{n}, \tag{11}$$

$$\sigma_S^2 = \frac{\sum_t (\mu_S - (I_t(i,j) - I_{t+1}(i,j))^2}{n-1}, \tag{12}$$

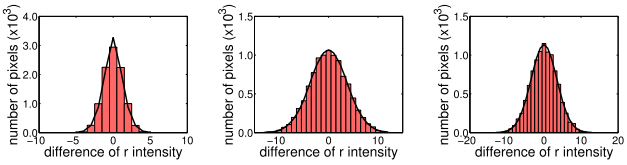

(a) Black (24th) (b) Gray (21st) (c) Red (15th)

Fig. 3. Skellam distribution estimated with 10,000 static images. The intensity difference follows a Skellam distribution well. (Larger images with more experimental results are available in the supplemental material, which can be found in the Computer Society Digital Library at http://doi.ieeecomputersociety.org/10.1109/TPAMI.2011.224.)

where $I_t(i,j)$ denotes the intensity at the (i,j) position at frame t, and n denotes the total number of images.

To investigate the Skellam parameters of various colors, we captured 10,000 static images of a GretagMacbeth ColorChecker using a Point Grey Scorpion camera (image $\text{resolution} = 1{,}600 \times 1{,}200$ pixels, exposure $\text{time} = 1/15$ s). Throughout this paper, we use raw camera data that are not demosaicked as we are dealing with the statistics of the raw intensity that is linearly proportional to the number of photons. Fig. 3 shows that the intensity difference follows the Skellam distribution closely, which confirms that our assumption of the dominant photon-dependent noise is appropriate. Parameters of the Skellam distribution differ according to a pixel color. As we expected, a black pixel has smaller Skellam parameters than a gray pixel, because $\mu^{(1)}$ and $\mu^{(2)}$ are the numbers of photons in the CCD cells during the capturing period.

As shown in Fig. 3, we applied our Skellam modeling scheme to a large number of static images. This modeling is possible using a single image of a color pattern by assuming that all pixels in the spatial domain are mutually independent. In other words, the noise distribution in the spatial domain is the same as that in the temporal domain. To verify this assumption, we compared noise parameters estimated in the spatial domain with those estimated in the temporal domain. We obtained the results in the temporal domain using (11) and (12). To estimate the noise in the spatial domain, we first selected image patches of the homogeneous color regions in the pattern image shown in Fig. 1a. Using these image patches, we applied our modeling strategy to the spatial domain using the following equations:

$$\mu_S = \frac{\sum_{(i,j)\in P}(I_t(i,j) - I_t(i+d_x, j+d_y))}{n}, \tag{13}$$

$$\sigma_S^2 = \frac{\sum_{(i,j)\in P}(\mu_S - (I_t(i,j) - I_t(i+d_x, j+d_y))^2}{n-1}, \tag{14}$$

where $(i,j) \in P$ denotes all the points in the patch, d_x and d_y represent disparities in the horizontal and vertical directions, respectively, and n denotes the total number of pixels in the patch. In this paper, d_x and d_y are set to one.

Fig. 4 shows the comparison between the modeling results in the spatial domain and those in the temporal domain. For this experiment, we used a HITACHI HV-F22 camera (3CCD, image $\text{resolution} = 1{,}280 \times 960$ pixels, exposure $\text{time} = 1/7.5$ s). The results shown in Fig. 4 verify that Skellam parameters estimated in the temporal and those

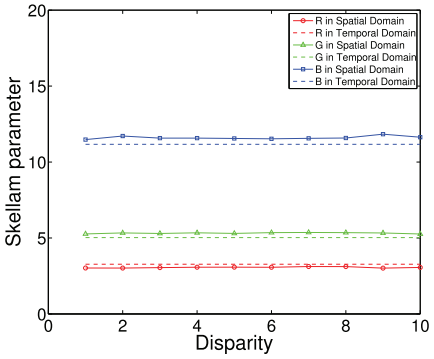

Fig. 4. Comparison of the Skellam parameters estimated in the spatial and in the temporal domains. Since the parameters from both domains are almost the same, intensity difference is an ergodic process.

estimated in the spatial domains are almost same. Thus, difference of intensity is an ergodic process; noise parameters estimated in temporal domain can be used in spatial analysis and vice versa. There are slight differences between the results in the temporal and spatial domains because we chose only one pixel in a patch in estimating the distribution in the temporal domain. Depending on which pixel is selected in a patch, its Skellam parameters vary slightly.

3.3 Skellam versus Gaussian

The distributions shown in Fig. 3 look similar to the zero-mean Gaussian distribution, and in this section we evaluate the two distributions, i.e., the proposed Skellam and the Gaussian quantitatively. To determine which distribution fits better to the actual data, we use a χ^2 test for goodness-of-fit (GOF), which is used to determine if a random sample is governed by a specific distribution [11]. In the χ^2 test for goodness-of-fit, we compute a measure for the given observed frequencies N_i and the expected frequencies e_i as

$$W = \sum_{i=1}^{r} \frac{(N_i - e_i)^2}{e_i}, \tag{15}$$

where r is the number of samples. Since the measure W follows a χ^2 distribution, the critical region C with a level of significance α in the hypothesis test is calculated by χ^2 statistics as

$$C = \{w : w \geq \chi^2_{\alpha,r-1}\}. \tag{16}$$

Therefore, if $W < \chi^2_{\alpha,r-1}$, the hypothesis that the expected distribution by the assumed model follows the actual observed distribution is accepted. We set $\alpha = 0.05$, the same as in [11].

We measured the goodness-of-fit for images captured by a Canon EOS-1D Mark III camera with low sensitivity $ISO100$. We captured a bright image and a dark image of the same scene as shown in Figs. 5a and 5c. For each patch, we estimate the distribution of the intensity difference by the Skellam and the Gaussian distributions. Figs. 5b and 5d show the test statistics for GOF from the modeling with the critical values $\chi^2_{\alpha,r-1}$, where r is the number of intensity levels in the histogram of each patch. Most of the modeling results using the Skellam distribution are less than the critical values as shown in Figs. 5b and 5d. It means that the hypothesis that noise distributions for color patches follow the Skellam distribution is acceptable. However, some

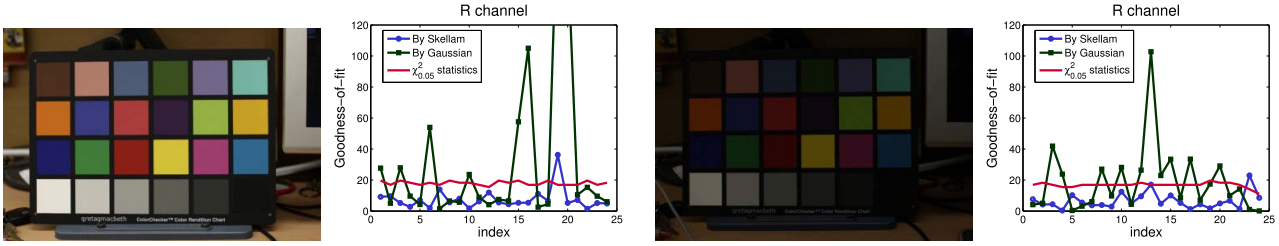

(a) a bright image (b) GOF in the bright image (c) a dark image (d) GOF in the dark image

Fig. 5. Comparison between the Skellam and Gaussian distributions by measuring goodness-of-fit in R channel of bright and dark images. The Skellam distribution explains an intensity difference better than the Gaussian distribution. (More results for other channels are available in the supplemental material, available online.)

modeling results by the Gaussian distribution exceed the critical values, and this shows that the intensity difference distribution is fitted better by the Skellam distribution than by the Gaussian distribution. Fig. 6 shows the comparison between Skellam and Gaussian distributions in two patches in Fig. 5a for intensity difference. As the GOF indicates in Fig. 5, a Skellam distribution explains the measured intensity difference better.

Though a Skellam distribution fits the measured intensity differences better than the Gaussian distribution, as we have shown above, it is possible to approximate the distribution as a Gaussian to utilize its advantages, such as its quadratic form, continuity, and differentiability. Note that, however, this does not mean that the intensity follows the additive Gaussian distribution, as we have shown in Fig. 1. Still, the direct modeling of the *intensity differences* is more accurate than the additive modeling of intensity, whichever parameterized distribution is chosen in explaining the intensity differences.

4 Noise Statistics Estimation Using Skellam Parameters

We have shown that Skellam distribution can explain intensity difference well, both in temporal and spatial domains. In this section, we will show that there is a useful relationship between pixel intensity and Skellam parameters, and we will make use of this relationship to easily estimate noise parameters in a single natural image.

4.1 Linearity between Intensity and Skellam Parameters

Under the assumption of a linear response camera, a linear relationship exists between pixel intensity and Skellam parameters $\mu^{(1)}$, estimated from intensity differences. Fig. 7 shows the scatter plot of an estimated Skellam parameter with respect to a sample mean of intensity measured in each patch for various cameras. As expected, the sample means and Skellam parameters are linearly related, and we call this line an intensity-Skellam line (ISL). We are able to estimate the Skellam parameters μ (that is, noise distribution) for each intensity value I from a given ISL, representing the ISL as

$$\mu^{(1)} = f_{ISL}(I) = R_{ISL} \cdot I + D_{ISL}, \tag{17}$$

where R_{ISL} is the ratio between intensity and the Skellam parameter and D_{ISL} is the Skellam parameter when expected intensity is zero, which refers to the dark current noise.

Theoretically, the line should change only according to camera gain, not scene radiance or illumination, because the camera gain dominantly determines the mapping from the number of photons to intensity. In other words, once an ISL of a camera has been determined, the line can be used for any image captured by the camera as long as the camera gain is maintained.

To validate this property, we captured multiple images using a Scorpion camera under various changes in camera aperture, illumination, and scene, while the camera gain is maintained, as shown in the left images of Fig. 8. We then manually selected homogeneous color patches of the ColorChecker in the images, and calculated Skellam parameters for each patch. The figure on the right in Fig. 8 is the scatter plot of all pairs of intensity and Skellam parameters. All the sample points using all the patches under various changes are on a single line, which means that the ISLs of all the images are the same. This result confirms that an ISL is independent of illumination, camera aperture, and scene.

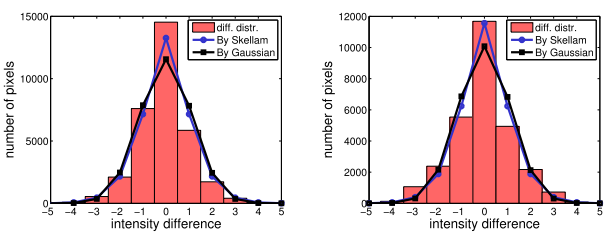

(a) 6th patch in Figure 5(a) (b) 16th patch in Figure 5(a)

Fig. 6. Comparison of fitting results by the Skellam distribution and the Gaussian distribution in R channel. As verified in Fig. 5, the fitting result by the Skellam distribution has a smaller discrepancy between the observed distribution and expected distribution.

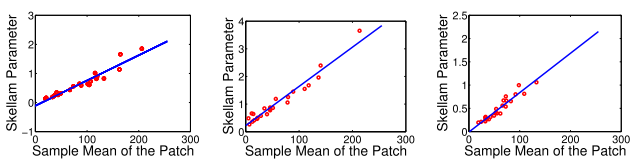

(a) R in HV-F22 (b) G in EOS 1D (c) B in C600

Fig. 7. Linearity between intensity and Skellam parameters for HITACHI HV-F22 (3-CCD camera), Canon EOS 1D (CMOS Consumer DSLR camera), and Logitech C600 (CMOS webcam). (Larger images with more results are available in the supplemental material, available online.)

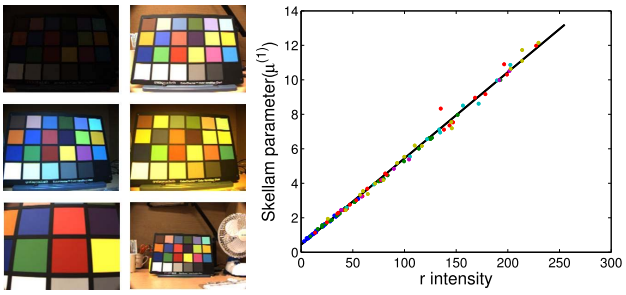

Fig. 8. Skellam parameters with respect to intensity under various illumination conditions and camera parameters, but fixed gain. Points in the same color are obtained in the same image. The ISL remains fixed when the camera gain is maintained.

We investigated the effect of camera gain to an ISL. Fig. 9a shows changes in the slope R_{ISL} and y-intercept D_{ISL} of an ISL with respect to camera gain. As expected, a slope R_{ISL} of an ISL is linearly proportional to a camera gain parameter. The y-intercept D_{ISL}, the amount of *dark current noise*, also increases as camera gain increases. We can represent the relationship between D_{ISL} and the camera gain using a simple parametric form, such as a second-order polynomial.

Another factor involved in taking a picture is exposure time. To see the effect of exposure time, we captured a series of images with increasing exposure time while keeping the camera gain constant. The figure on the left in Fig. 9b shows the relationship between the ISL slope and exposure time. As exposure time increases, the slope of the ISL remains nearly constant; its variance is within 0.002. This is expected because the relationship between intensity and the number of photons does not change as exposure time varies. The figure on the right in Fig. 9b shows that the magnitude of dark current noise D_{ISL} increases as exposure time increases because longer integration time increases the amount of dark current noise. Note that the change of D_{ISL} with respect to exposure time is much smaller than that with respect to camera gain. In practice, this change of D_{ISL} with respect to exposure time is negligible. If necessary, especially in the case of extremely long exposure time, the relationship between exposure time and dark current noise can also be represented in a parametric form, and the ISL parameters for a given exposure time can be determined from these parametric representation.

To sum up the results of these experiments, the ISL is invariant under changes of environment and camera parameters, as shown in Fig. 8, except under changes of camera gain and exposure time. However, we can determine the ISL parameters even under these changes, once we have parametric representations of the ISL changes with respect to the gain and exposure time. The parametric representation can be easily obtained using measurements like those shown in Fig. 9. In many practical cases, it is sufficient to consider only the effect of gain, and not that of exposure time.

This linearity between intensity and a Skellam parameter is useful in estimating noise distributions. Ideally, only two pairs of intensity-Skellam parameters are enough to define a line, although we generally use more—10 or 20—for robustness. Once the ISL is determined, noise distribution

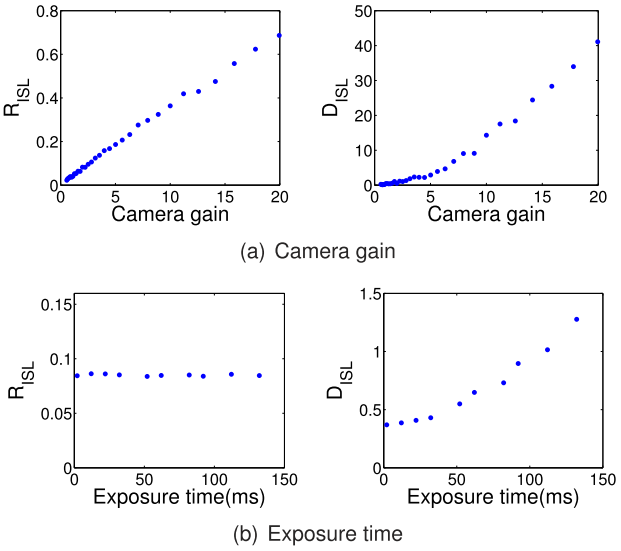

Fig. 9. Relationship of ISL parameters to camera gain and exposure time. The ISL parameters under varying camera gain and exposure time can be represented in a parametric form.

can be obtained for any intensity value in any image captured by the camera unless its gain changes.

4.2 Estimation of Intensity-Skellam Lines Using a Single Natural Image

Estimation of an ISL requires homogeneous color patches, as illustrated by the line fitting shown in Fig. 7. However, finding a homogeneous patch in a natural image is not trivial. Conventional approaches use color segmentation to locate homogeneous regions [2], [3], but the segmentation is not trivial either.

Instead, we use the properties of Skellam parameters to select appropriate patches. The Skellam mean is calculated as the mean of the difference between intensity of neighboring pixels in (13). Transition of colors between neighboring pixels causes a big shift in the Skellam mean in the color transition. When the patch contains color transition, the Skellam mean increases sharply. Consequently, we can collect homogeneous patches to estimate the ISL by checking if their Skellam means are around zero.

When an image is captured under directional illumination, the Skellam mean of a homogeneous patch may be shifted slightly. To accommodate this, we first construct a histogram of Skellam means. By localizing a peak in the

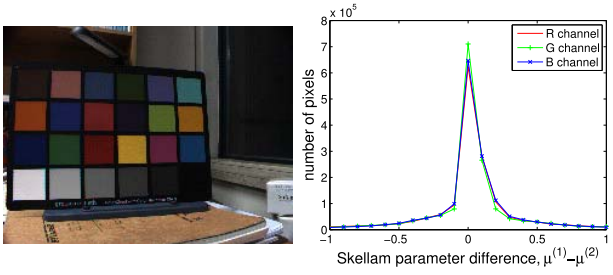

(a) Test image (b) Histogram of $\mu^{(1)} - \mu^{(2)}$

Fig. 10. Histogram of the Skellam mean $\mu^{(1)} - \mu^{(2)}$. Skellam means of homogeneous patches are close to zero, and a natural image tends to have a strong peak in the histogram of Skellam means.

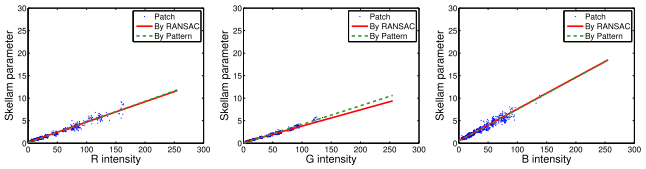

(a) R channel (b) G channel (c) B channel

Fig. 11. ISL estimation using a single natural image. The proposed automatic patch selection method provides ISL parameters similar to those estimated by manually picked patches in the color pattern image.

histogram of Skellam means, the mean shift effect can be considered. Fig. 10b shows the histogram of Skellam means for the input image of Fig. 10a. Although illumination was located above the scene, the mean of estimated Skellam parameters shifted only slightly in our experiments.

We can easily localize the peak in the Skellam parameter difference and then use patches that find a Skellam mean close to the peak. However, pairs of intensity and Skellam parameters for the patches are not exactly on a single line because of Skellam parameter variation. In addition, some outliers may not be removed by the simple filtering using the peak of the histogram. To alleviate these problems, we apply a simple RANSAC algorithm to determine a line. Fig. 11 shows the estimation result using 1,000 19×19 patches. We randomly selected the patches to reduce time complexity. For comparison, we show the line obtained from manually segmented color patterns. The ISLs automatically estimated using a natural image are close to those estimated using manually selected patches on the pattern image.

4.3 Determining an Intensity Acceptance Range

Now we have noise distributions based on intensity differences, and we can use the data to statistically test if an intensity difference comes from sensor noise or from different signals. Our strategy for determining this *intensity acceptance range* is to test a hypothesis of difference on the distribution (or to find confidence intervals) given a confidence level.

To test a hypothesis, we use a cumulative distribution function (cdf). Because the pmf of a Skellam distribution is defined only at integer values, the cdf is calculated as

$$F(K;\mu^{(1)},\mu^{(2)}) = \sum_{k=-\infty}^{K} e^{-(\mu^{(1)}+\mu^{(2)})}\left(\frac{\mu^{(1)}}{\mu^{(2)}}\right)^{k/2} I_{|k|}(2\sqrt{\mu^{(1)}\mu^{(2)}}). \quad (18)$$

The acceptance region for a critical value I is

$$A(I) = \{v|v < I\} = F\big(I;\mu^{(1)},\mu^{(2)}\big) - F\big(-I;\mu^{(1)},\mu^{(2)}\big). \quad (19)$$

We determine the intensity acceptance range I_A, i.e., the critical value, as

$$I_A = \arg\max_I A(I) \quad \text{s.t. } A(I) \le 1-\alpha, \quad (20)$$

where α is the size of the type I error, which is a true rejection rate with confidence level $(1-\alpha)*100\%$ [11].

One of the advantages of the proposed modeling is that the noise statistics are only dependent on camera gain. Thus, unless this gain changes, it is possible to determine in advance a range of intensity variations caused by sensor noise. By calculating the intensity acceptance range for each intensity value, we can build a look-up table of ranges. Once we have a look-up table of precomputed confidence intervals for a camera setting, we do not need to test a hypothesis for each pixel every time.

5 Background Subtraction in Temporal Domain

In Section 4, we have an accurate noise distribution for each pixel in the image. In the temporal domain, background subtraction, which compares a current image to a background image, is a good example for using the proposed difference-based noise modeling.

For applications using temporal domain analysis of two or more images, a probabilistic framework is usually adopted to model the uncertainty of temporal changes including image noise. For foreground extraction, variance of intensity for each pixel can be described using a multimodal distribution. Stauffer and Grimson [12] used a mixture of Gaussians as an intensity distribution, and Elgammal et al. [13] proposed a method using a nonparametric kernel estimation by building a histogram of intensity values. However, their probabilistic modeling may fail to estimate the distribution by image noise accurately without the direct consideration of noise characteristics.

5.1 Background Subtraction Strategy

For each pixel, the noise distribution statistically tells us whether the color difference between the background and a current pixel comes from a foreground change or from sensor noise. Classification is then performed by a statistical hypothesis test [11], or by simply looking up the intensity acceptance range table in Section 4.3. This algorithm is extremely simple, involving a set of per-pixel operations: calculating the difference between two intensity values and comparing the difference with the intensity acceptance range value in a look-up table. Unlike other methods [13], we do not need any further processing because our noise modeling is so precise that subtraction results have few false alarms, as shown in Fig. 12.

In addition, the background update algorithm becomes simpler than those for other methods since the foreground estimation result is very accurate. We update the background only when there is no interframe change in consecutive T frames. This approach is feasible thanks to the highly accurate change detection between each consecutive frame.

5.2 Background Subtraction Results

We applied our algorithm to outdoor sequences captured in bright and dark environments. We used a Point Grey Flea camera with 640×480 resolution. Fig. 12a shows the results in a bright environment; the leftmost and subsequent images are the current and background images, respectively. Foreground detection results were so accurate that our method was able to detect nearly true boundaries for moving people and cars. Compared with the results obtained by the mixture of Gaussians [12], results obtained

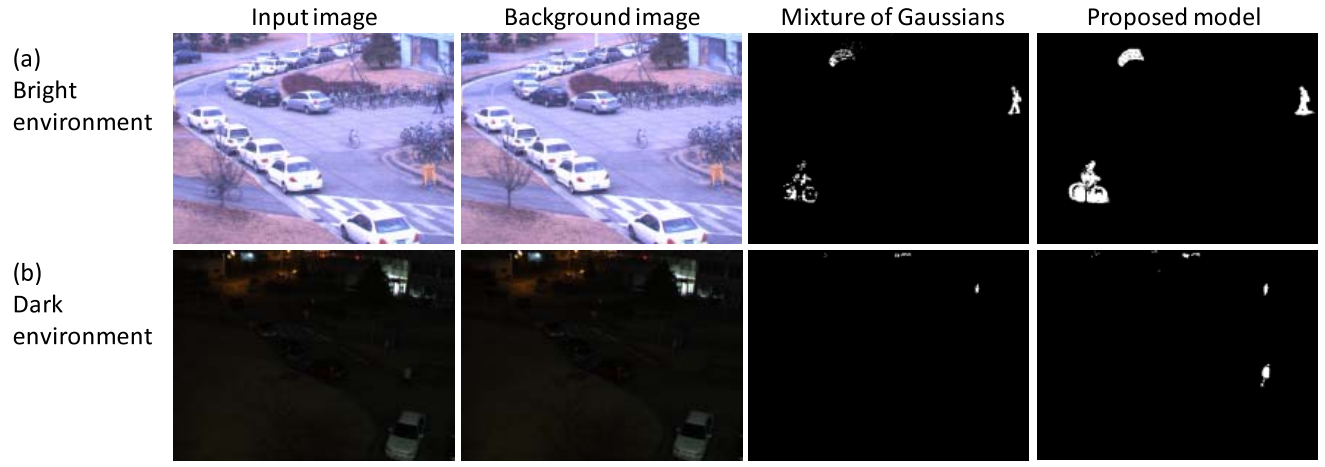

Fig. 12. Background subtraction results. The proposed method works robustly even in the complex background and a dark environment. (Additional larger results are available in the supplemental material, available online.)

with our difference-based noise modeling provided much smaller misses in spite of complex backgrounds. This is because the mixture of Gaussians cannot guarantee an exact distribution of pixel color differences, but instead provides merely rough approximation of Gaussian distributions for background estimation.

In Fig. 12b, we present the foreground detection results in a dark environment. The sequence was captured outdoors at 9 p.m. Since the images are very dark, detection of moving objects is not easy, even by human vision. Intensity variation of the changed regions in this dark environment was much lower than that in the bright environment. Therefore, exact noise distribution for classifying foreground pixels was essential in this situation. The proposed method was able to detect moving objects well because each pixel had an exact distribution according to intensity. The method that used the mixture of Gaussians failed to detect most of moving objects due to overfitting of the background model. The overfit model includes not only temporal color changes of the background, but also color changes of the foreground, which makes it hard to discriminate foreground pixels from it.

In Table 1, we make a quantitative comparison using manually selected ground truth. Because the proposed method is sensitive to the signal change, it generates fewer false negatives than the mixture of Gaussians. Though the proposed method seems to generate more false positives than the mixture of Gaussians, almost all the false positives are near the shadow region, which shows the sensitivity of the proposed model to intensity changes. Note that the performance of the proposed model is not significantly degraded for the dark images without any parameter change. All the ground-truths and experimental results are provided in the supplemental material, available online.

6 Edge Detection in Spatial Domain

We apply our noise modeling to edge detection as a spatial domain application. Most edge detectors smooth an image using Gaussian kernels to suppress the image noise. However, the edge detector based on our noise model does not smooth images because the proposed algorithm presents the exact ranges of intensity variations caused by sensor noise.

6.1 Noise Handling for Feature Detection

For applications based on a single image, most approaches do not model image noise explicitly in the spatial domain, but suppress image noise as a preprocessing step. The

TABLE 1
Performance Comparison Using Ground-Truths

Scene	Method	False negatives	False positives	Total errors
Bright scene 1	MoG	2166/5783 (37.45%)	257/301417 (0.08%)	2423/307200 (0.79%)
	Proposed	726/5783 (12.55%)	874/301417 (0.29%)	1600/307200 (0.52%)
Bright scene 2	MoG	4702/7126 (65.98%)	199/300074 (0.06%)	4901/307200 (1.60%)
	Proposed	1495/7126 (20.98%)	745/300074 (0.25%)	2240/307200 (0.73%)
Bright scene 3	MoG	958/1713 (55.93%)	62/305487 (0.02%)	1020/307200 (0.33%)
	Proposed	439/1713 (25.63%)	229/305487 (0.07%)	668/307200 (0.22%)
Dark scene 1	MoG	1243/1310 (94.89%)	18/305890 (0.005%)	1261/307200 (0.41%)
	Proposed	494/1310 (37.71%)	182/305890 (0.05%)	676/307200 (0.22%)
Dark scene 2	MoG	759/960 (79.06%)	61/306240 (0.02%)	820/307200 (0.27%)
	Proposed	284/960 (29.58%)	124/306240 (0.04%)	408/307200 (0.13%)
Dark scene 3	MoG	672/679 (98.97%)	4/306521 (0.001%)	676/307200 (0.22%)
	Proposed	435/679 (64.07%)	47/306521 (0.015%)	482/307200 (0.15%)
Total	MoG	72.047%	0.031%	0.603 %
	Proposed	31.753%	0.119%	0.328%

The proposed method generated fewer false negatives than the mixture of Gaussians while maintaining low false positive rates.

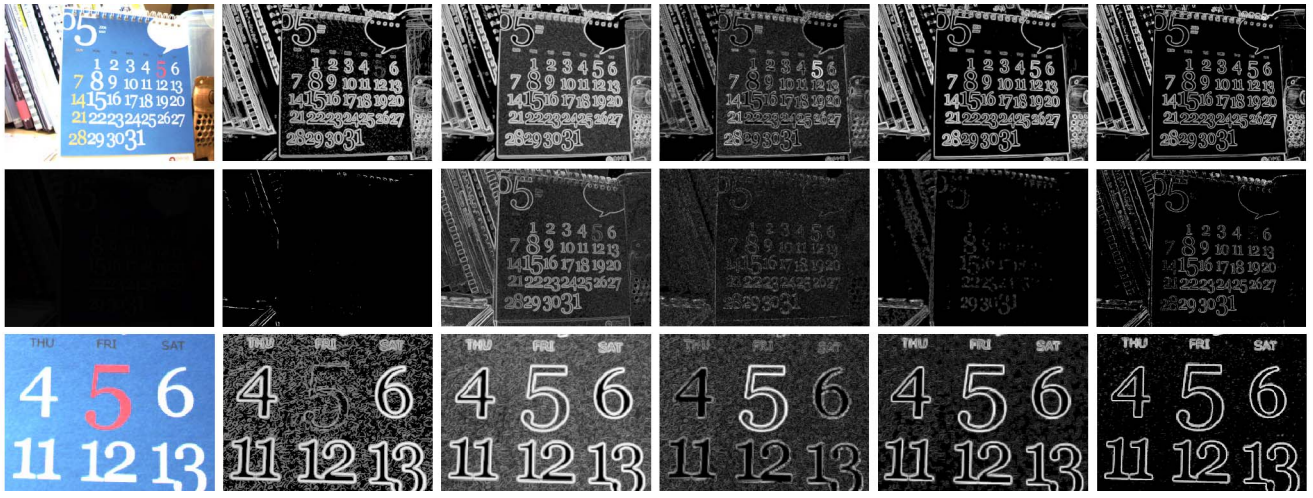

Fig. 13. Log-normalized edge measures under various illumination conditions: From the left, input image, Canny edge response, RGB gradient magnitude, quasi-invariants [14], generalized compass operator [15], and the proposed edge measure. The proposed edge measure suppresses the noise while preserving edges even in the very dark image without changing any parameters. (Larger images are available in the supplemental material, available online.)

conventional strategy for extracting features such as a corner and an edge is to preprocess the images using Gaussian kernels to suppress the image noise via smoothing [14], [17]. A linear filtering method, such as Gaussian smoothing, basically cuts off high-frequency components of signals as a low-pass filter, and it suppresses the important abrupt changes of the signals as well as noise. Consequently, features usually defined by the high frequency are affected by the filtering: rounded corners, disconnected T-junctions, and displacements of features near intensity gradients [18]. To minimize this effect, filtering adaptive to the local structure can be used [19], but it loses one of the key advantages of the computational efficiency of the Gaussian smoothing by its linear separability. Although the parameters of Gaussian smoothing must be determined properly, the effects of the parameters have been considered in only a few studies [19].

6.2 Edge Detection Strategy

Our strategy for edge detection is similar to that for background subtraction. When the difference between two neighboring pixels is within the intensity acceptance range, there is no edge; otherwise, there is an actual change of scene colors, which implies an edge.

Magnitudes of derivatives in horizontal and vertical directions at (i, j) are defined as

$$\left|d_x^c(i,j)\right| = |I^c(i-1,j) - I^c(i+1,j)|, \tag{21}$$

$$\left|d_y^c(i,j)\right| = |I^c(i,j-1) - I^c(i,j+1)|, \tag{22}$$

where I^c is an intensity value in the color channel c, which is one of r, g, and b in RGB color space. Then, edge measures in horizontal and vertical directions are defined as

$$e_x^c(i,j) = \begin{cases} \dfrac{\left|d_x^c(i,j)\right| - I_A}{I_A}, & \text{if } \left|d_x^c(i,j)\right| \geq I_A, \\ 0, & \text{if } \left|d_x^c(i,j)\right| < I_A, \end{cases} \tag{23}$$

$$e_y^c(i,j) = \begin{cases} \dfrac{\left|d_y^c(i,j)\right| - I_A}{I_A}, & \text{if } \left|d_y^c(i,j)\right| \geq I_A, \\ 0, & \text{if } \left|d_y^c(i,j)\right| < I_A, \end{cases} \tag{24}$$

where I_A denotes the intensity acceptance range, as determined in Section 4.3 of the intensity $I^c(i,j)$. This edge measure calculates the normalized distance of the intensity $I^c(i,j)$ from the intensity acceptance range I_A. If the magnitude of a derivative is within the range I_A, the edge measure is zero. The total edge measure of a pixel is obtained by summing all the horizontal and vertical edge measures as

$$e(i,j) = \sum_c e_x^c(i,j) + \sum_c e_y^c(i,j). \tag{25}$$

Only when all the horizontal and vertical edge measures of a pixel are zero is the pixel regarded as a nonedge pixel. This method preemptively suppresses an edge response caused by sensor noise.

Once edge measures for all pixels are calculated, we apply nonmaximum suppression. In [17], two values are required for a hysteresis threshold to link edges after nonmaximum suppression. However, we regard the pixels that have nonzero edge measures as being edge pixels because the intensity difference exceeds the intensity acceptance range determined from the noise distribution. Thus, we do not discard nonzero edge pixels when generating a final edge image.

6.3 Edge Detection Results

In the first experiment, we show the independent property of the proposed method to the brightness and illumination. We do not change the parameters of each detector for images captured by the same camera. Fig. 13 shows log-normalized edge measures under various illumination conditions in order to observe weak responses participating in the edge linking. We compared the results of the proposed method with a 99 percent confidence level to those of other edge operators. Our difference-based method suppresses the noise properly and detects edges even in very dark environments without changing any parameters.

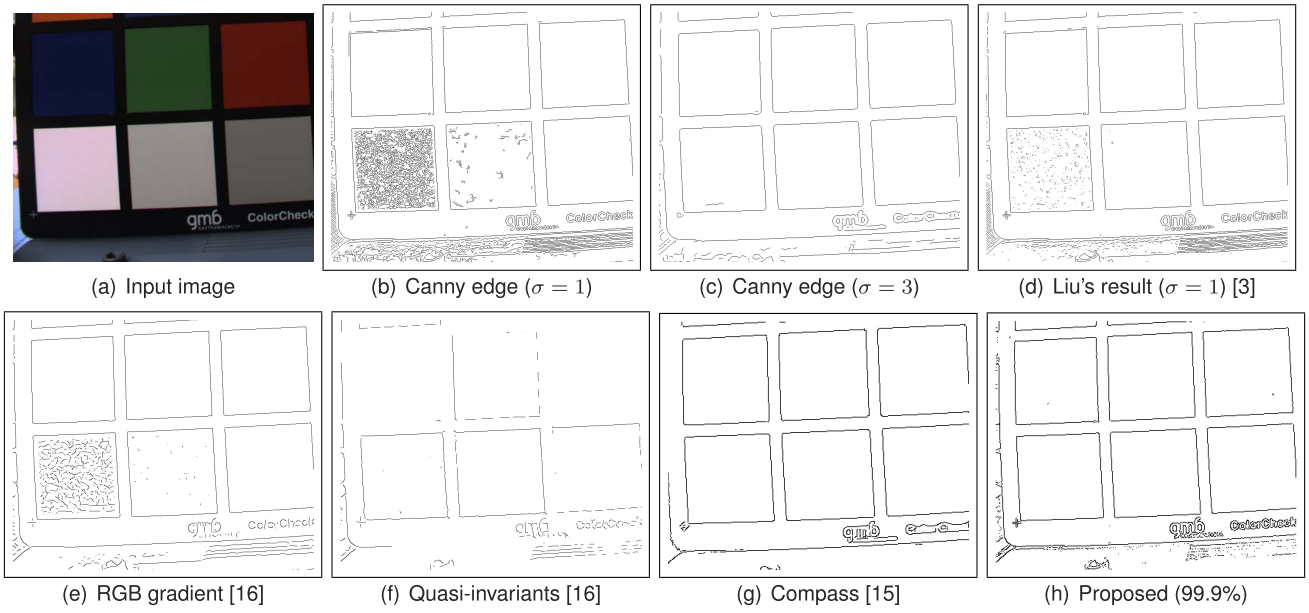

(a) Input image (b) Canny edge ($\sigma = 1$) (c) Canny edge ($\sigma = 3$) (d) Liu's result ($\sigma = 1$) [3]

(e) RGB gradient [16] (f) Quasi-invariants [16] (g) Compass [15] (h) Proposed (99.9%)

Fig. 14. Edge detection results. The proposed method provides good noise suppression without image smoothing. (More results are available in the supplemental material, available online.)

Using the parameter for the first image, the Canny operator does not detect the details under dark illumination (the second image) and does not suppress the false edges caused by image noise (the third image), which means that the parameter should be carefully chosen for each image. We also compared the proposed difference-based edge detector to other existing color edge detectors, i.e., RGB gradient magnitude, shadow-shading-specular quasi-invariants [14], and generalized compass operator [15], using MATLAB codes provided by the authors. Color gradient and quasi-invariant methods provided large responses by image noise, which can result in many false alarms, even under normal illumination condition. Results by the quasi-invariant method also show poor connectivity of edge measures, resulting in many short edges after edge linking. The generalized compass operator worked well under the normal illumination, but did not generate responses in the dark image and made some responses based on noise.

Fig. 14 shows the final results of the proposed edge detection after nonmaximum suppression and binarization, compared with other edge detectors. Conventional edge detectors [17] require user-defined tuning parameters for image smoothing and edge linking, which are not easy to determine. Liu's method [3] statistically chooses the thresholds of the Canny method, but a user still needs to determine a proper smoothing filter. The color tensor based edge detectors [16] and the compass operator [15] requires a proper smoothing scale as well. Unlike the conventional edge detectors, the proposed edge detector does not smooth images, but successfully suppresses the image noise while preserving the fine details, as shown in Fig. 14.

We have also compared the Skellam and signal dependent Gaussian distributions for an intensity difference in the edge detection task, as shown in Fig. 15. The input image was captured by a Point Grey Flea camera with a low noise level and long exposure time. The only difference between Figs. 15b and 15c is the distribution for intensity difference. The Skellam distribution for intensity difference suppresses the image noise successfully, while the Gaussian distribution does not, by underestimating the thresholds for each intensity. This shows that the Skellam distribution can explain the intensity difference better than the Gaussian distribution for edge detection.

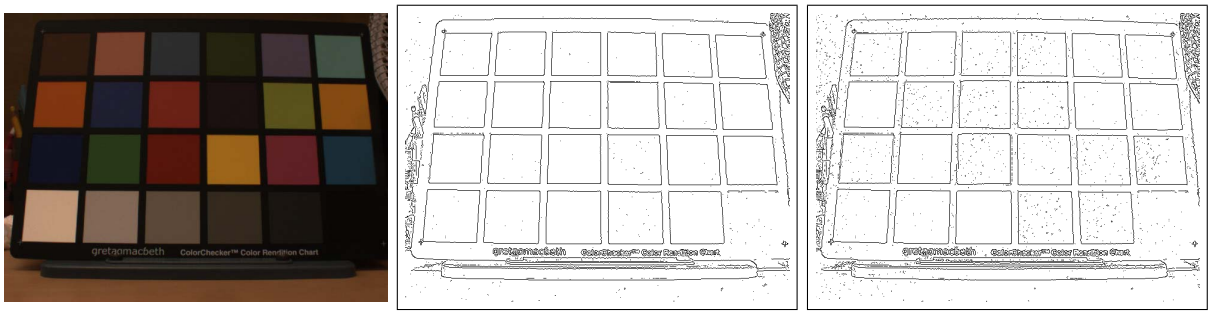

(a) Input image (b) Skellam distribution (c) Gaussian distribution

Fig. 15. Results of the edge detection with 99.9 percent confidence intervals using the proposed Skellam distribution and its signal-dependent Gaussian approximation for intensity difference. The Gaussian distribution underestimates the threshold values and does not suppress the image noise fully.

7 Conclusion

In this paper, we propose to directly model intensity difference for determining whether two intensity values come from the same radiance or not. The pixel intensity should be expressed as a random variable, and the conventional additive model may not explain the intensity distribution due to the laws of quantum physics and illumination effects. We have presented some examples of the wrong assumptions of the conventional models, and verify that the direct modeling of intensity difference can be a better way to model the image noise.

We also present a Skellam distribution for a linear response camera derived from the dominant photon noise assumption. The validity has been checked thoroughly with various cameras under various camera settings and illumination conditions. We have found that the level of intensity difference is the same in the spatial and in the temporal domains, and this property enables us to use a single image for the modeling. In addition, there exists a strong linear relationship between the intensity and the Skellam parameters measured in images even under the natural illumination. This difference-based model is only dependent on the camera gain, not on the scene, illumination, and aperture. Once it is obtained, the noise level of the other intensity values can be determined simply. These properties make the sensor noise process much easier than the previous methods. The difference of two intensity values can be tested on every pixel by statistical tests based on the obtained distribution of intensity difference.

To show the validity of the proposed intensity difference model, we applied it to background subtraction in the temporal domain and to edge detection in the spatial domain. In background subtraction, foreground pixels can be accurately detected using per-pixel operations based on the intensity acceptance range. Because per-pixel detection is accurate, further process to refine the result is not required. In the spatial domain, we design a simple color edge detector in the same way of background subtraction. Without any smoothing or filtering, the edge detector based on the intensity difference model suppresses image noise, while it detects the actual radiance changes well in both dark and bright images.

As we presented in this paper, the proposed noise model can be used to detect meaningful signal changes robustly to the image noise. Further works include development of image denoising, feature detection, and optical flow estimation robust to the image noise.

Acknowledgments

This research is supported by the National Research Laboratory (NRL) program (No. M1-0302-00-0064) of the Ministry of Science and Technology (MOST) and the National Research Foundation of Korea (NRF) grant funded by the Korea government (MEST) (No. 2011-0018250).

References

[1] F. Alter, Y. Matsushita, and X. Tang, "An Intensity Similarity Measure in Low-Light Conditions," *Proc. European Conf. Computer Vision,* pp. 267-280, 2006.

[2] C. Liu, R. Szeliski, S.B. Kang, C.L. Zitnick, and W.T. Freeman, "Automatic Estimation and Removal of Noise from a Single Image," *IEEE Trans. Pattern Analysis and Machine Intelligence,* vol. 30, no. 2, pp. 299-314, Feb. 2008.

[3] C. Liu, W.T. Freeman, R. Szeliski, and S.B. Kang, "Noise Estimation from a Single Image," *Proc. IEEE Conf. Computer Vision and Pattern Recognition,* pp. 901-908, 2006.

[4] G.E. Healey and R. Kondepudy, "Radiometric CCD Camera Calibration and Noise Estimation," *IEEE Trans. Pattern Analysis and Machine Intelligence,* vol. 16, no. 3, pp. 267-276, Mar. 1994.

[5] A. Foi, M. Trimeche, V. Katkovnik, and K. Egiazarian, "Practical Poissonian-Gaussian Noise Modeling and Fitting for Single-Image Raw-Data," *IEEE Trans. Image Processing,* vol. 17, pp. 1737-1754, Oct. 2008.

[6] M. Yavuz and J.A. Fessler, "Maximum Likelihood Emission Image Reconstruction for Randoms-Precorrected PET Scans," *Proc. IEEE Nuclear Science Symp. Conf. Record,* pp. 15/229-15/233, 2000.

[7] Y. Hwang, J.-S. Kim, and I.-S. Kweon, "Sensor Noise Modeling Using the Skellam Distribution: Application to the Color Edge Detection," *Proc. IEEE Conf. Computer Vision and Pattern Recognition,* 2007.

[8] I. Young, J. Gerbrands, and L. van Vliet, "Image Processing Fundamentals," *The Digital Signal Processing Handbook,* V.K. Madisetti, D.B. Williams, eds., pp. XI-1-XI-81, CRC Press, 1997.

[9] J.G. Skellam, "The Frequency Distribution of the Difference between Two Poisson Variates Belonging to Different Populations," *J. Royal Statistical Soc.: Series A,* vol. 109, no. 3, p. 296, 1946.

[10] M. Abramowitz and I.A. Stegun, *Handbook of Mathematics Functions with Formulas, Graphs, and Mathematical Tables.* Dover, 1972.

[11] E.R. Dougherty, *Probability and Statistics for the Engineering, Computing and Physical Sciences.* Prentice Hall, 1990.

[12] C. Stauffer and W. Grimson, "Learning Patterns of Activity Using Real-Time Tracking," *IEEE Trans. Pattern Analysis and Machine Intelligence,* vol. 22, no. 8, pp. 747-757, Aug. 2000.

[13] A. Elgammal, D. Harwood, and L. Davis, "Non-Parameteric Model for Background Subtraction," *Proc. European Conf. Computer Vision,* pp. 751-767, 2000.

[14] J. Weijer, T. Gevers, and J. Geusebroek, "Edge and Corner Detection by Photometric Quasi-Invariants," *IEEE Trans. Pattern Analysis and Machine Intelligence,* vol. 27, no. 4, pp. 625-630, Apr. 2005.

[15] M.A. Ruzon and C. Tomasi, "Edge, Junction, and Corner Detection Using Color Distributions," *IEEE Trans. Pattern Analysis and Machine Intelligence,* vol. 23, no. 11, pp. 1281-1295, Nov. 2001.

[16] J.V.D. Weijer, T. Gevers, and A.W.M. Smeulders, "Robust Photometric Invariant Features from the Color Tensor," *IEEE Trans. Image Processing,* vol. 15, no. 1, pp. 118-127, Jan. 2006.

[17] J. Canny, "A Computational Approach to Edge Detection," *IEEE Trans. Pattern Analysis and Machine Intelligence,* vol. 8, no. 6, pp. 679-698, Nov. 1986.

[18] A. Blake and A. Zisserman, *Visual Reconstruction.* The MIT Press, 1987.

[19] P. Saint Marc, J. Chen, and G. Medioni, "Adaptive Smoothing: A General Tool for Early Vision," *IEEE Trans. Pattern Analysis and Machine Intelligence,* vol. 13, no. 6, pp. 514-529, June 1991.

Youngbae Hwang received the BS, MS, and PhD degrees in electrical engineering and computer science from KAIST in 2001, 2003, and 2009, respectively. He is currently a senior researcher at Korea Electronics Technology Institute (KETI). After six months as a post-doctoral researcher for KAIST, he worked for the Robot Business Group at Samsung Techwin as a senior research engineer for one and a half years. His research interests include image noise modeling, low-level processing, video surveillance, 3D reconstruction, and robot localization. He is a member of the IEEE.

Jun-Sik Kim received the BS degree in electronic engineering from Yonsei University in 1999, and the MS and PhD degrees in electrical engineering and computer science from KAIST in 2001 and 2006, respectively. He is currently a project scientist at Carnegie Mellon University. After about one year as a postdoctoral researcher for KAIST, he worked for the Robotics Institute at Carnegie Mellon University as a postdoctoral fellow for two years. His research interests include camera calibration, 3D reconstruction, camera motion tracking, sensor fusion, image sensor noise modeling, and acceleration using parallelized hardwares. He is a member of the IEEE.

In So Kweon received the BS and MS degrees in mechanical design and production engineering from Seoul National University, Seoul, Korea, in 1981 and 1983, respectively, and the MS and PhD degrees in robotics from the Robotics Institute, Carnegie Mellon University, Pittsburgh, Pennsylvania, in 1986 and 1990, respectively. He worked for Toshiba R&D Center, Japan, and joined the Department of Automation and Design Engineering, KAIST, Seoul, Korea, in 1992, where he is now a professor with the Department of Electrical Engineering. His research interests are in computer vision, robotics, pattern recognition, and automation. Specific research topics include invariant-based visions for recognition and assembly, 3D sensors and range data analysis, color modeling and analysis, robust edge detection, and moving object segmentation and tracking. He is a member of ICASE and the ACM. He is a member of the IEEE.